---

**Article:**
Ogasawara, Takahiro, Jackson, Edward Alan, Tsunoda, Masakiyo et al. (2 more authors) (2019) In-plane and perpendicular exchange bias effect induced by an antiferromagnetic D019 Mn2FeGa thin film. Journal of Magnetism and Magnetic Materials. pp. 307-312. ISSN 0304-8853

https://doi.org/10.1016/j.jmmm.2019.04.024

---

Journal of Magnetism and Magnetic Materials 484 (2019) 307–312

Contents lists available at ScienceDirect

Journal of Magnetism and Magnetic Materials

journal homepage: www.elsevier.com/locate/jmmm

Research articles

# In-plane and perpendicular exchange bias effect induced by an antiferromagnetic $D0_{19}$ $Mn_2FeGa$ thin film

Takahiro Ogasawara[a,b,*], Edward Jackson[b], Masakiyo Tsunoda[c,e], Yasuo Ando[a,d,e], Atsufumi Hirohata[b,*]

[a] Department of Applied Physics, Graduate School of Engineering, Tohoku University, Sendai 980-8579, Japan
[b] Department of Electronic Engineering, University of York, Heslington YO10 5DD, United Kingdom
[c] Department of Electronic Engineering, Graduate School of Engineering, Tohoku University, Sendai 980-8579, Japan
[d] Center for Science and Innovation in Spintronics (Core Research Cluster) Organization for Advanced Studies, Tohoku University, Sendai 980-8577, Japan
[e] Center for Spintronics Research Network, Tohoku University, Sendai 980-8577, Japan

ABSTRACT

Fe-doped $D0_{19}$ $Mn_3Ga$ films were studied in terms of both their in-plane and perpendicular exchange bias field, $H_{ex}$, induced in the attached ferromagnetic layer. The $(Mn,Fe)_3Ga$ films were deposited on a Si substrate with a Ru buffer layer with a (0 0 0 1)-oriented single $D0_{19}$ phase at room temperature. Consequently, in-plane and perpendicular $H_{ex}$ were measured in bilayers with a CoFe layer and a [Co/Pt] multilayer, respectively. In-plane $H_{ex}$ was found to be dependent on the Fe compositions, showing the largest value of 446 Oe at 120 K for 10-nm-thick $Mn_{1.99}Fe_{0.41}Ga$. Perpendicular $H_{ex}$ was dependent on not only the Fe compositions but also the thickness of $(Mn,Fe)_3Ga$, exhibiting the maximum of 163 Oe at 120 K for 5-nm-thick $Mn_{1.96}Fe_{0.67}Ga$. The median blocking temperature of both in-plane and perpendicular $H_{ex}$ systems for 10-nm-thick $(Mn,Fe)_3Ga$ were measured to be 235 and 240 K, respectively. The measured in-plane and perpendicular $H_{ex}$ induced by $(Mn,Fe)_3Ga$ are generated by a spin structural change from noncollinear to noncoplaner in *ab*-plane as expected from the previous theoretical study [A. Kundu and S. Ghosh, *Intermetallics* **93**, 209 (2018)].

## 1. Introduction

Exchange bias effect induced at the interface between a ferromagnet and an antiferromagnet was discovered in 1965 [1] and has been studied intensively especially for the practical spintronics applications, such as magnetoresistive random access memory (MRAM) and magnetic sensors [2–6]. As these devices are based on the spin-dependent transport using tunnel magnetoresistance (TMR) [7,8] or giant magnetoresistance (GMR) [9,10], it is required to pin the magnetization of a reference layer along one direction to realize well-defined parallel and antiparallel configurations of the magnetizations in the two ferromagnetic layers. For this purpose, exchange biased ferromagnet/antiferromagnet bilayers, which are then inserted into a spin valve structure for GMR and TMR [11], has been playing a key role for magnetoresistive multilayers towards device applications.

From the view point of antiferromagnetic materials, IrMn is the most commonly used material to induce the exchange bias because of a high exchange field, $H_{ex}$ generated in the neighbouring ferromagnet and thermal robustness. However, new antiferromagnetic materials need to be explored in order to replace IrMn, as Ir has been recognized as a critical raw material [12,13]. Consequently, Mn-based cubic ($L2_1$, $B_2$ and $A_2$ phases) Heusler antiferromagnets, *i.e.*, $Mn_2YZ$ structure, have been investigated in accordance with the generalized Slater-Pauling relationship [14], which allows us to compensate net spin moments by selecting $Y$ and $Z$ atoms appropriately. As a result, the exchange bias, a shift in a hysteresis loop, has been reported using cubic $Mn_2VSi$ [15] and $Mn_2VAl$ [16] films. On the other hand, when a $Mn_2MnZ$ Heusler alloy is distorted along the (1 1 1) direction, its crystalline structure is known to be changed from cubic ($L2_1$, $B_2$ and $A_2$ phases) to hexagonal $D0_{19}$ ($Ni_3Sn$ type with the space group of P63/mmc) [17] with Mn triangular moments forming a Kagome lattice [18,19] which is magnetically stabilized by the Dzyaloskinskii-Moriya interaction [20,21]. Hence, noncollinear antiferromagnets with the structure of $Mn_3Z$ ($Z$ = Ga, Ge and Sn) have been widely investigated [22–24]. Although the mechanism of the exchange bias effect is still under discussion, hexagonal $Mn_3Z$ ($Z$ = Ga [13,25–27], Ge [28] and Sn [29]) alloys have a tendency to demonstrate a large exchange bias and higher blocking temperature, $T_B$, in their film form when compared to cubic $Mn_2YZ$ [15,16]. In our previous work, 10-nm-thick $D0_{19}$ $Mn_3Ga$ grown by high target utilization sputtering (HiTUS) showed in-plane $H_{ex}$ of 299 Oe at 120 K and average blocking temperature, $< T_B >$, of 235 K which is higher than our previous study on the cubic $Mn_2VSi$ film grown by the same method [15]. Furthermore, by optimizing growth conditions using sputtering, a very large in-plane $H_{ex}$ of 1.5 kOe at room

* Corresponding authors at: Department of Applied Physics, Graduate School of Engineering, Tohoku University, Sendai 980-8579, Japan (T. Ogasawara).
*E-mail addresses:* takahiro.ogasawara.p3@dc.tohoku.ac.jp (T. Ogasawara), atsufumi.hirohata@york.ac.uk (A. Hirohata).

https://doi.org/10.1016/j.jmmm.2019.04.024
Received 1 March 2019; Received in revised form 3 April 2019; Accepted 8 April 2019
Available online 13 April 2019

temperature and $T_B$ of 648 K were achieved in 10-nm-thick $D0_{19}$ $Mn_3Ga$ [24]. Since these antiferromagnetic properties are comparable to IrMn, $Mn_3Ga$ can be one of the promising candidates for the replacement of IrMn.

In recent years, regarding the great potential of perpendicular magnetic anisotropy (PMA) owing to high thermal stability and integration density, perpendicularly exchange biased systems are desirable for magnetic memory applications. Perpendicular exchange bias was firstly demonstrated in CoO in contact with a [Co/Pt] multilayer [30]. Afterwards, FeMn [31], NiO [32], IrMn [33] and MnN [34] were found to induce a perpendicular exchange bias for a [Co (CoFe)/Pt] multilayer or CoFeB with PMA. According to the discussion by S. Maat et al. [30], the projection of the perpendicular spin anisotropy axis from the film plane in antiferromagnetic CoO gives rise to a perpendicular exchange bias. In other words, perpendicular components of a spin alignment in an antiferromagnet is of considerable significance for the observation of the perpendicular exchange bias. Recently, spin configuration of $D0_{19}$ $Mn_2FeGa$, which is formed from $D0_{19}$ $Mn_3Ga$ by the partial Fe replacement of Mn, was studied by first principles calculations [35]. In their calculation, a stable spin configuration is found to be changed from triangular in the *ab*-plane for $Mn_3Ga$ to collinear like in the *ab*-plane for $Mn_2FeGa$ whilst maintaining the $D0_{19}$ structure. Moreover, the total energies in coplanner and noncoplanar spin configurations along the *ab*-plane are estimated to be almost the same. This theoretical result suggests the magnitude of the in-plane or out-of-plane exchange bias can be controlled by the Fe doping into $Mn_3Ga$ with the corresponding spin structural changes. In this paper, we investigate $(Mn,Fe)_3Ga/(Co_{0.6}Fe_{0.4}$ or [Co/Pt]) bilayer systems with different Fe concentrations and discuss the effect of Fe doping into $D0_{19}$ $Mn_3Ga$ in terms of their in-plane and perpendicular exchange bias.

## 2. Experimental procedure

All of the films were prepared using the HiTUS system with a base pressure less than $5 \times 10^{-5}$ Pa. The samples with the stacking structure of Ta (5)/Ru (35)/$(Mn,Fe)_3Ga$ (*t*)/$Co_{0.6}Fe_{0.4}$ (3.3) or [Co (1.0)/Pt (1.6)]$_3$/Ta (5) and Ta (5)/Ru (35)/$(Mn,Fe)_3Ga$ (50)/Ta (5) (thickness in nm) were sputtered on Si (0 0 1) substrates in Ar atmosphere of 0.186 Pa at room temperature. For convenience, hereinafter, we denote Fe-doped $Mn_3Ga$ as $(Mn,Fe)_3Ga$. Also, experimental film compositions of $(Mn,Fe)_3Ga$ are described as $Mn_xFe_yGa$, where *x* and *y* is the composition of Mn and Fe against Ga, respectively. The ferromagnetic layers of CoFe or [Co/Pt] multilayers were used to measure the in-plane or perpendicular exchange bias, respectively. The $(Mn,Fe)_3Ga$ compositions were controlled by adding Fe pegs on a $Mn_3Ga$ target, which were measured to be $Mn_{1.98}Fe_{0.41}Ga$, $Mn_{1.99}Fe_{0.49}Ga$, $Mn_{1.96}Fe_{0.67}Ga$, $Mn_{1.96}Fe_{0.75}Ga$, $Mn_{1.94}Fe_{0.86}Ga$ and $Mn_{1.90}Fe_{1.10}Ga$ by energy dispersive X-ray spectroscopy (EDX; Thermo Scientific, UltraDry). The crystalline structures were determined using a X-ray diffraction (XRD; Rigaku, Smart Lab) at room temperature. Also, magnetic properties were measured using a vibrating sample magnetometer (VSM; ADE, Model 10) and a superconductive quantum interface device (SQUID; Quantum Design) at elevating range of temperatures from 100 to 400 K. In-plane or perpendicular exchange bias was induced before the measurement by field annealing under an in-plane or perpendicular external magnetic field.

## 3. Results

Fig. 1(a) shows XRD diffraction patterns of 2$\theta$ scans for the films of Ta (5)/Ru (35)/$(Mn,Fe)_3Ga$ (*t*)/Ta (5) with different compositions. This 50-nm-thick $(Mn,Fe)_3Ga$ films were only used for XRD measurement in order to increase the signal intensity. It exhibits clear peaks of (0 0 0 2) and (0 0 0 4) $D0_{19}$ $(Mn,Fe)_3Ga$ for all the compositions. $Mn_3Ga$ has two stable crystalline structures of $D0_{19}$ antiferromagnetic and $D0_{22}$ ferrimagnetic phases as previously reported [36], however no minor peaks

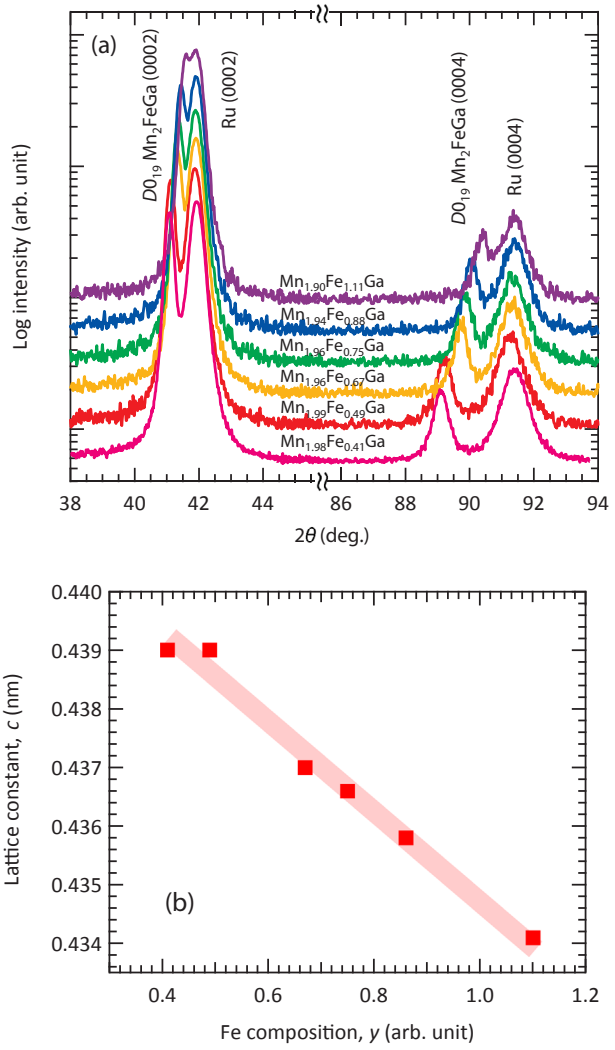


**Fig. 1.** (a) XRD diffraction patterns of 50-nm-thick $(Mn,Fe)_3Ga$ films with different Fe compositions. (b) Lattice constant, *c*, as a function of Fe composition, *y*, in $Mn_xFe_yGa$ films.

from $D0_{22}$ phases are detected in the Fe-doped films, which indicates that Fe-doped $Mn_3Ga$ have successfully grown with a single (0 0 0 1)-oriented $D0_{19}$ phase. The peak shifts of (0 0 0 2) and (0 0 0 4) prove the effect of the Fe doping on the reduction in the lattice constants. From their peak positions, the lattice constant of *c* is estimated as summarized in Fig. 1(b). This graph shows that *c* becomes smaller with increasing Fe composition, *y*, which agrees well with the previous theoretical calculations of the decrease in *c*-axis lattice constant from 0.426 nm in $Mn_3Ga$ [17] to 0.420 nm in $Mn_2FeGa$ [35]. Experimentally, a lattice constant of bulk $D0_{19}$ $Mn_2FeGa$ is measured to be $a = 0.5315$ nm and $c = 0.4305$ nm [37], where *c* is smaller than our $Mn_{1.90}Fe_{1.10}Ga$ film with 0.4341 nm. This difference is expected to be brought from a lattice mismatch of $-1.6\%$ with the Ru buffer layer, resulting in a minor lattice distortion to $Mn_2FeGa$.

Fig. 2(a) and (b) show magnetization curves of 50-nm-thick $Mn_{1.98}Fe_{0.41}Ga$ and $Mn_{1.90}Fe_{1.10}Ga$ measured at room temperature. $D0_{19}$ $Mn_3Ga$ are reported to show weak ferromagnetism with small net moments of 0.015 $\mu_B$ per Mn in the bulk form [38]. In our case, saturation magnetization, $M_s$, of $Mn_{1.98}Fe_{0.41}Ga$ and $Mn_{1.90}Fe_{1.10}Ga$ are measured to be 15 and 20 emu/cm$^3$, respectively. These values correspond to 0.023 and 0.030 $\mu_B$ per Mn, respectively, which are larger than the bulk study of $Mn_3Ga$ [38]. However, net moments of $Mn_3Z$ in the film forms have been reported to become larger than that in the bulk

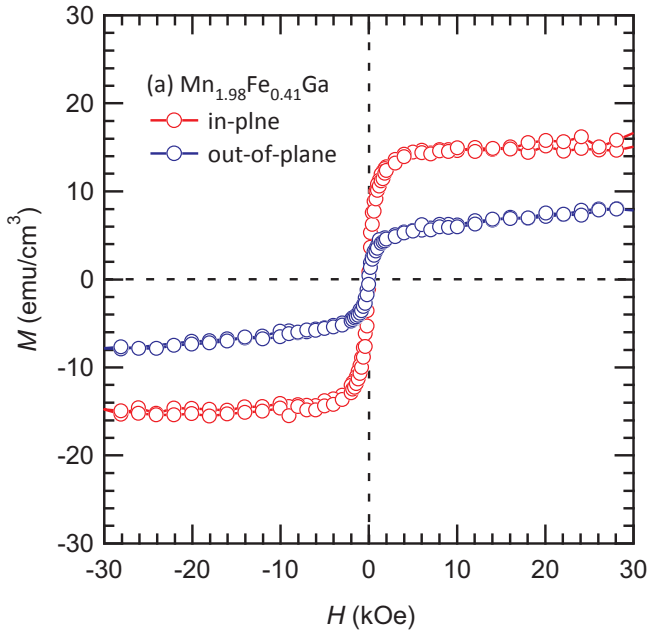


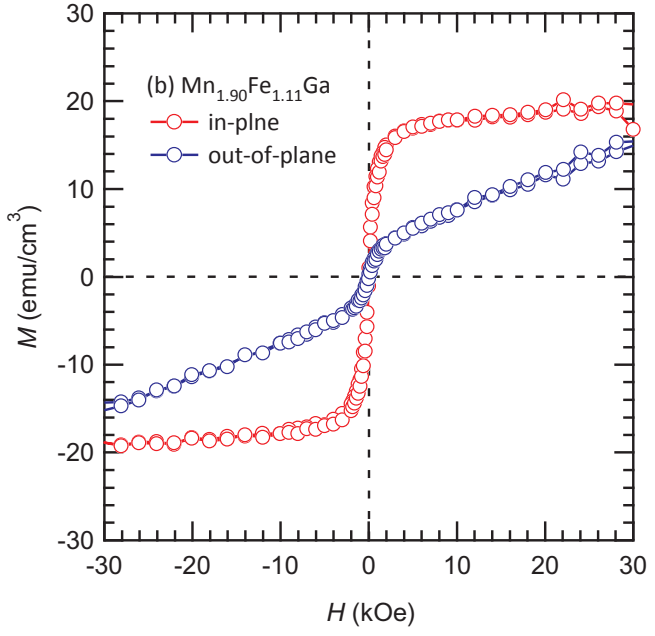


**Fig. 2.** Magnetization curves of 50-nm-thick (a) $Mn_{1.98}Fe_{0.41}Ga$ and (b) $Mn_{1.90}Fe_{1.11}Ga$ films measured at room temperature.

form, for example, 34 emu/cm$^3$ for both $D0_{19}$ $Mn_3Ge$ [28] and $Mn_3Sn$ [29] thin films. Therefore, we believe our measured values are in reasonable agreement with the previous reports. The increase of $M_s$ in the Fe-rich film is associated with the deformation of triangular Mn atoms. Furthermore, magnetization curves with an out-of-plane magnetic field are changed from the ones with an in-plane field for the films with $Mn_{1.98}Fe_{0.41}Ga$ and $Mn_{1.90}Fe_{1.10}Ga$, which indicates the modification of the magnetic anisotropy of weak ferromagnetic properties. A perpendicular magnetic anisotropy constant, $K_u^{eff}$ is estimated to be *ca.* $-4.8 \times 10^5$ and $-3.1 \times 10^5$ erg/cm$^3$ for $Mn_{1.98}Fe_{0.41}Ga$ and $Mn_{1.90}Fe_{1.10}Ga$, respectively from their magnetization curves. This decrease of magnetic anisotropy magnitude also supports the spin structural change from the in-plane to perpendicular direction with increasing Fe concentration of $(Mn,Fe)_3Ga$ films.

Firstly, we discuss an in-plane exchange bias. Fig. 3 shows in-plane

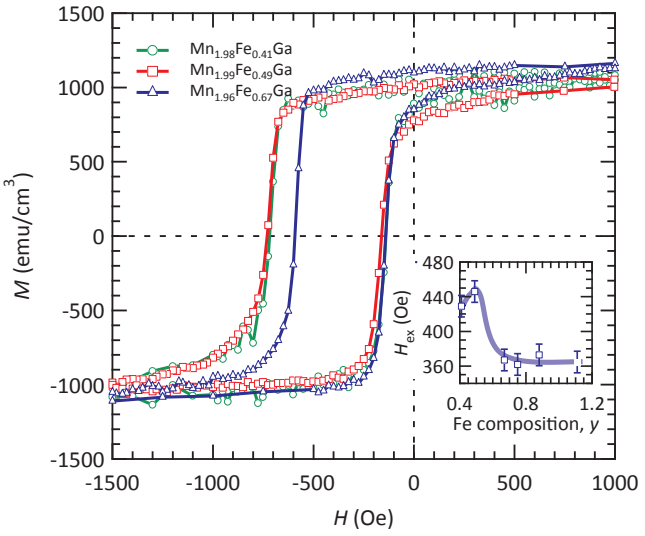


**Fig. 3.** In-plane magnetization curves of $(Mn,Fe)_3Ga$ (10)/CoFe (3.3) bilayers with different Fe compositions at 120 K after field annealing at 500 K for 30 min. The inset shows the Fe composition dependence of the in-plane exchange bias.

magnetization curves of $Mn_2FeGa$ (10)/CoFe (3.3) films measured at 120 K after field annealing at 500 K for 30 min. The horizontal shift of the magnetization curves indicates the presence of the exchange coupling between $(Mn,Fe)_3Ga$ and $Co_{0.6}Fe_{0.4}$ layers in each compositions. The magnitude of the in-plane exchange bias values, $H_{ex}^{in\text{-}plane}$, is varied depending on the Fe compositions. The inset of Fig. 3 summarizes the change of $H_{ex}^{in\text{-}plane}$ as a function of Fe composition, $y$. A clear enhancement of exchange bias is achieved at $y = 0.49$, showing the largest $H_{ex}^{in\text{-}plane}$ of 446 Oe at 120 K which is greater than our previous work on $Mn_{2.80}Ga$ (10)/CoFe (3.3) film with $H_{ex}$ of 299 Oe at 120 K [11]. On the other hand, $H_{ex}^{in\text{-}plane}$ becomes saturated to *ca.* 360 Oe in the regime of $y > 0.67$. In addition, the vertical shift of the magnetization curve is seen for all the compositions, which implies the presence of uncompensated spins at the interface of ferromagnet and antiferromagnet [39,40]. The amount of uncompensated spins is known to be proportional to the vertical shift and is known to increase the exchange bias [41]. In our case, the vertical shifts for $Mn_{1.98}Fe_{0.41}Ga$ and $Mn_{1.99}Fe_{0.49}Ga$ are measured to be 49 and 35 emu/cm$^3$, respectively, while the exchange bias for $Mn_{1.98}Fe_{0.41}Ga$ (429 Oe) is smaller than $Mn_{1.99}Fe_{0.49}Ga$ (446 Oe). This implies that uncompensated spins do not predominantly contribute to the $H_{ex}$ enhancement in our samples.

Instead, interfacial roughness between the ferromagnet and antiferromagnet can contribute to the change in the saturation magnetization as an exchange bias is an interfacial effect. Fig. 4 shows X-ray reflectivity (XRR) signals for all the Fe compositions. An XRR oscillation decay can reflect interfacial roughness of the films. As can be seen in Fig. 4, all the films display similar decaying behavior, which suggests that interfacial roughness is almost consistent independent of the Fe composition. We estimated the roughness at the $(Mn,Fe)_3Ga/Co_{0.6}Fe_{0.4}$ interfaces to be 0.5 nm. Therefore, we attribute the $H_{ex}^{in\text{-}plane}$ modification not to uncompensated spins or to interfacial roughness but predominantly to the spin structural change in $Mn_2FeGa$ by the Fe doping as discussed in Ref. [35].

In polycrystalline films, from microscopic viewpoints, exchange bias properties can vary in each antiferromagnetic grains whose range of sizes follow a lognormal distribution [42]. Therefore, we carried out median blocking temperature, $< T_B >$, measurements by following the York Protocol [43]. Previous studies on polycrystalline films reveal that the exchange bias can be induced only by medium-sized grains because too large (or small) antiferromagnetic grains have too high (or low)

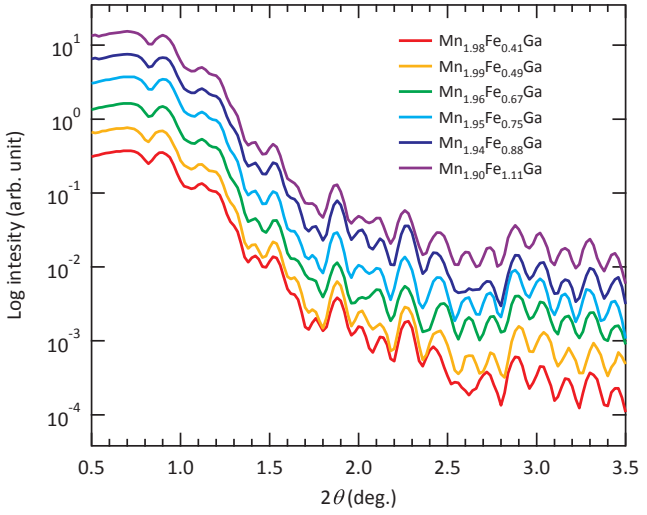


**Fig. 4.** X-ray reflectivity of $(Mn,Fe)_3Ga$ (10)/CoFe (3.3) bilayers with different Fe compositions.

energy barriers to be set by the field annealing, therefore not exhibiting exchange bias. In our measurement, the samples were annealed at 400 K for 90 min under an external magnetic field of 20 kOe and cooled down to 100 K to induce the exchange bias in medium-sized grains. After this process, the samples were heated up to a thermal activation temperature of $T_{act}$ for 30 min under a magnetic field of −20 kOe to reverse the antiferromagnetic ordering in some grains, which is called a thermal activation procedure. Corresponding magnetization curves after each thermal activation procedure were measured at 100 K. $T_{act}$ was elevated from 100 to 400 K in our measurements.

Fig. 5(a) shows magnetization curves of the $Mn_{1.99}Fe_{0.49}Ga$ (10)/CoFe (3.3) film measured at 100 K after the thermal activation at 100, 200, 250 and 350 K. At $T_{act}$ = 100 K, a negative shift is confirmed due to the field annealing under a positive magnetic field as expected. With increasing $T_{act}$, the $H_{ex}$ values are changed gradually from negative to positive, which is caused by reversed antiferromagnetic ordering by the thermal activation since higher $T_{act}$ can reverse the antiferromagnetic ordering in the larger grains. Fig. 5(b) shows the evolution of $H_{ex}^{in\text{-}plane}$ after the thermal activation at elevated $T_{act}$. When $H_{ex}^{in\text{-}plane}$ becomes zero, half of the set grains in a lognormal distribution are expected to be reversed. This temperature is called the median blocking temperature, $< T_B >$. In this film, $< T_B >$ is estimated to be 235 K which is the same as our previous 10-nm-thick $Mn_3Ga$ film [27]. As mentioned above, it is theoretically predicted that spin structure of $D0_{19}$ $Mn_3Ga$ and $Mn_2FeGa$ are changed from triangular to collinear like structure along *ab*-plane by Fe doping [35]. However, this spin structural difference do not bring a significant change for antiferromagnetic anisotropy in our samples, which results in the same $< T_B >$ of 235 K between Fe-doped and un-doped $D0_{19}$ $Mn_3Ga$.

Secondly, we characterize the perpendicular exchange bias, $H_{ex}^{perp}$, in $(Mn,Fe)_3Ga$/$[Co(1.0)/Pt(1.6)]_3$ structures. Fig. 6 shows out-of-plane magnetization curves of $Mn_{1.98}Fe_{0.41}Ga$ and $Mn_{1.96}Fe_{0.67}Ga$ with perpendicularly magnetized $[Co(1.0)/Pt(1.6)]_3$ layers measured at 120 K after field annealing at 500 K for 30 min. From the clear horizontal loop shifts, perpendicular exchange bias is induced by $Mn_2FeGa$. The $H_{ex}^{perp}$ values are varied depending on the Fe compositions. For $y$ = 0.49, although $H_{ex}^{perp}$ of 109 Oe is the smallest, $H_{ex}^{perp}$ increases for larger Fe compositions and roughly saturates in the range $y > 0.67$. The largest $H_{ex}^{perp}$ that is achieved is 150 Oe at $y$ = 0.67. Fig. 7 shows the interfacial exchange coupling energy, $J_{ex}$, with increasing Fe composition for the cases of in-plane and perpendicular anisotropy. $J_{ex}$ are calculated using the equation, $J_{ex} = H_{ex}M_s t_F$, where $H_{ex}$ is the value of exchange bias measured, $M_s$ and $t_F$ are the saturation magnetization and thickness of ferromagnetic layer, respectively. For the case of the in-plane

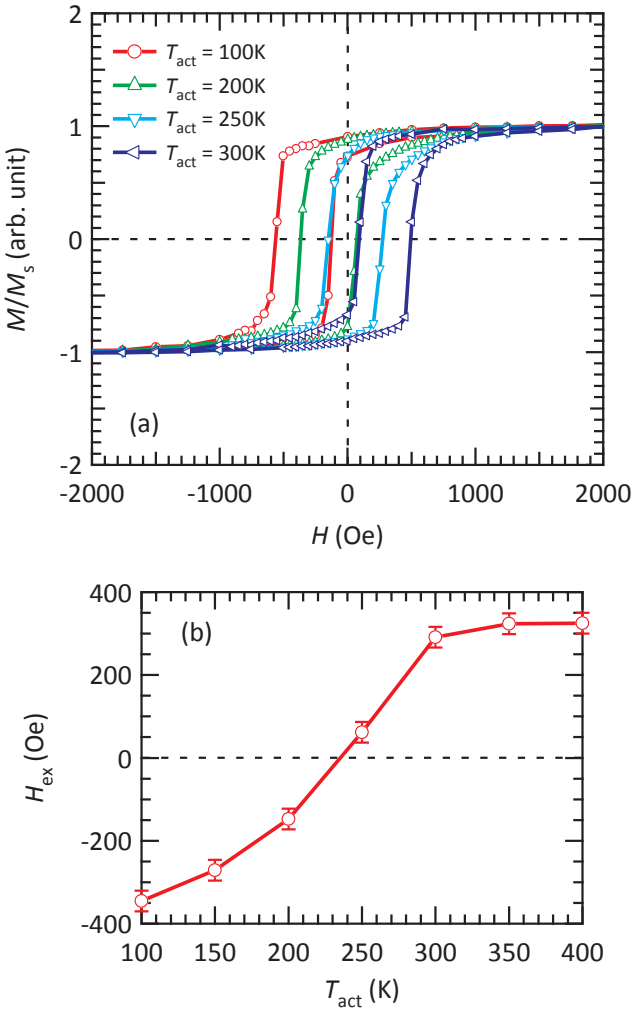


**Fig. 5.** (a) In-plane magnetization curves of the $Mn_{1.99}Fe_{0.49}Ga$ (10)/CoFe (3.3) bilayer measured at 100 K after thermal activation at different $T_{act}$ under a reversed magnetic field. (b) $H_{ex}^{in\text{-}plane}$ dependence on $T_{act}$.

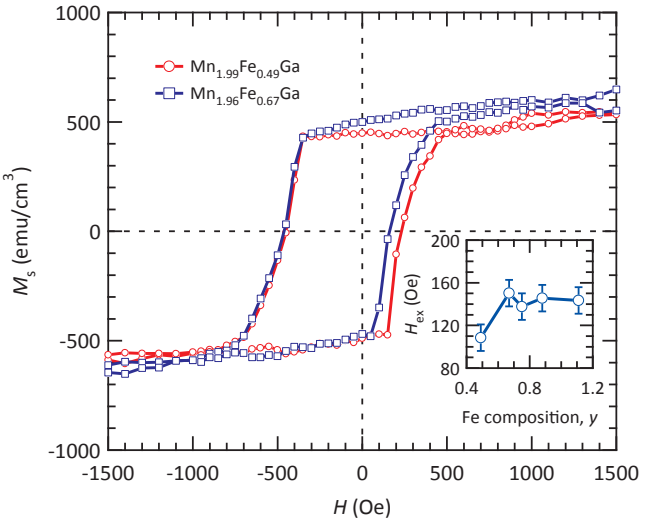


**Fig. 6.** Out-of-plane magnetization curves of $(Mn,Fe)_3Ga$ (10)/$[Co(1.0)/Pt(1.6)]_3$ bilayers with different Fe compositions at 120 K after field annealing at 500 K for 30 min. The inset shows the Fe composition dependence of the perpendicular exchange bias.

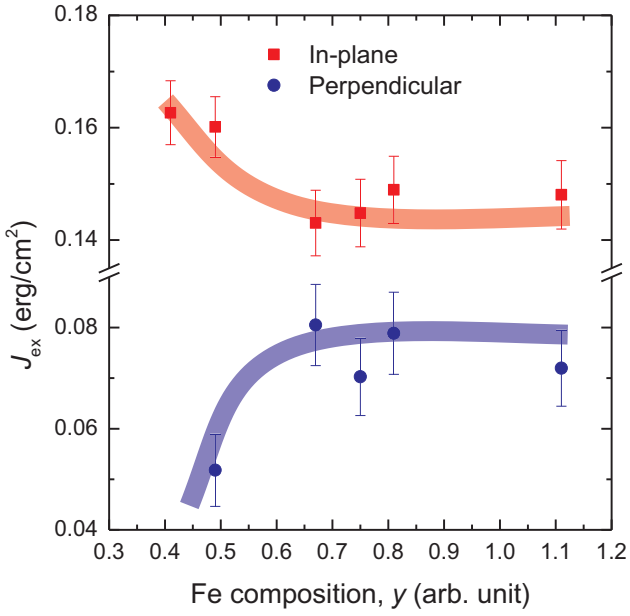


**Fig. 7.** $J_{ex}$ dependence of $(Mn,Fe)_3Ga$ with different Fe composition for in-plane and perpendicular exchange bias at 120 K.

anisotropy, $J_{ex}^{in\text{-}plane}$ shows relatively larger values at low Fe compositions with the largest values of 0.163 erg/cm$^2$. $J_{ex}^{in\text{-}plane}$ then decreases monotonically within $0.49 < y < 0.67$ and becomes saturated above $y = 0.67$. For the case of the perpendicular anisotropy, on the other hand, $J_{ex}^{perp.}$ shows a smaller values at low Fe concentration. However, it increases to 0.081 erg/cm$^2$ at $y = 0.69$ and becomes saturated above $y = 0.67$. Note that $J_{ex}$ depends on a ferromagnet as well as an antiferromagnet. In our samples with both in-plane and perpendicular anisotropy, the values of $J_{ex}$ as shown above are calculated with the adjacent ferromagnets of $Co_{60}Fe_{40}$ and Co ([Co/Pt]) for the in-plane and perpendicular anisotropy, respectively. M. Tsunoda et al. reported the CoFe composition dependence for $J_{ex}$, revealing that $J_{ex}$ in $Co_{0.6}Fe_{0.4}$ is larger than that in Co [44] Therefore, the difference of the magnitude of $J_{ex}$ between the in-plane and perpendicular anisotropy can be induced by the different ferromagnetic layers attached for these samples but the opposite behavior with respect to the Fe concentration is important finding to reveal the spin structure of $D0_{19}$ $Mn_2FeGa$. In addition, according to the report by S. Maat et al. [30], the $J_{ex}$ dependence of $y$ reflects the fact that antiferromagnetic spins of $Mn_2FeGa$ are aligned in the *ab*-plane with small Fe dopant concentrations. With increasing Fe doping, on the other hand, the easy axis of antiferromagnetic spin configurations, which lies between the *ab*-plane and the *c*-axis depending on their micromagnetic energy, may be changed gradually from noncollinear to noncoplanar. Our findings agree with the calculation of spin formation energy in $D0_{19}$ $Mn_2FeGa$ [35]. It should be noted that even if the stable spin structure is in the *ab*-plane, the perpendicular field annealing is believed to assist the setting of the antiferromagnetic ordering along the perpendicular direction as long as perpendicular spin components exist. The critical Fe concentration of spin structure changes is estimated to be around $0.49 < y < 0.67$ in our films because both $H_{ex}^{in\text{-}plane}$ and $H_{ex}^{perp}$ show significant changes in this range. Both $J_{ex}$ are saturated for $y > 0.67$, indicating that the spin structural change is completed beyond the critical Fe dopant concentration.

Next, we investigate the thickness dependence of $H_{ex}^{perp}$. Fig. 8 shows out-of-plane magnetization curves of $Mn_{1.96}Fe_{0.67}Ga$ $(t)$/[Co (1.0)/Pt(1.6)]$_3$ at 120 K after field annealing at 400 K for 30 min. The $Mn_{1.96}Fe_{0.67}Ga$ film is used since it is the optimized composition to induce the largest $H_{ex}^{perp}$ as shown in Fig. 6. As shown in Fig. 8, as $t$ becomes thinner, $H_{ex}^{perp}$ is found to increase, similarly to the case of

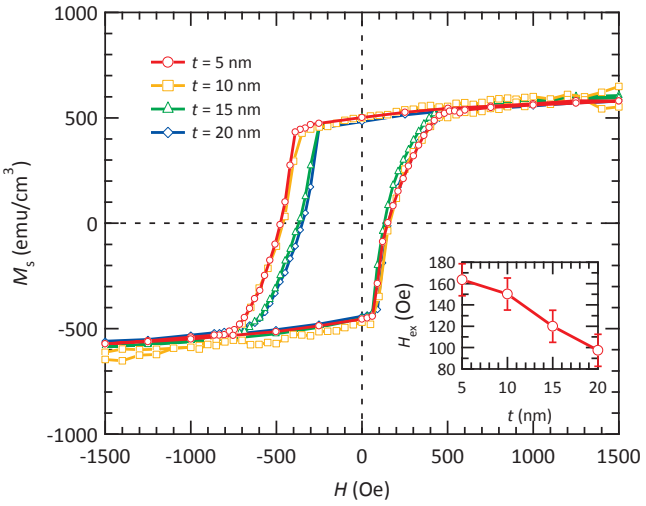


**Fig. 8.** Out-of-plane magnetization curves of $Mn_{1.96}Fe_{0.67}Ga$ $(t)$/[Co(1.0)/Pt (1.6)]$_3$ bilayers measured at 120 K after field annealing at 500 K for 30 min. The inset shows the thickness dependence of the perpendicular exchange bias.

$H_{ex}^{in\text{-}plane}$ of $Mn_3Ga$ [27]. Consequently, $H_{ex}^{perp}$ has a maximum of 163 Oe when $t = 5$ nm whereas it is 98 Oe at 20 nm. If the spin structure is changed depending on the thickness, in-plane and perpendicular $H_{ex}$ must be in the trade-off relationship as a function of the thickness, however, both in-plane [27] and perpendicular $H_{ex}$ increase with decreasing thickness of $Mn_3Ga$ or $Mn_2FeGa$. Therefore, we conclude that the spin structure is almost unchanged as the $Mn_2FeGa$ thickness is carried whereas the change of interfacial condition, antiferromagnetic anisotropy and grain sizes may contribute to the enhancement of $H_{ex}$. Although there may be a critical thickness below 5 nm of $(Mn,Fe)_3Ga$ which the exchange bias disappears due to the minimum thickness required for crystallisation, our finding that the large $H_{ex}$ is induced with the thin antiferromagnetic layer is favorable for device implementation to reduce the total thickness.

Fig. 9(a) shows out-of-plane magnetization curves of $Mn_{1.96}Fe_{0.67}Ga$ (10)/[Co (1.0)/Pt (1.6)]$_3$ bilayer measured at 100 K by following the York Protocol after thermal activation at $T_{act}$ = 100–325 K. Similarly to $H_{ex}^{in\text{-}plane}$ as seen in Fig. 5, the loop shift from a negative to positive magnetic field is observed in the out-of-plane magnetization curves with increasing $T_{act}$. Fig. 9(b) shows the evolution of $H_{ex}^{perp}$ in the samples of $Mn_{1.96}Fe_{0.67}Ga$ (5, 10)/[Co (1.0)/Pt (1.6)]$_3$ after the thermal activation at elevated $T_{act}$, resulting in $< T_B >$ to be estimated as 185 and 240 K for 5 and 10-nm-thick $Mn_{1.96}Fe_{0.67}Ga$, respectively. From this graph, as increasing $T_{act}$, $H_{ex}^{perp}$ of 5-nm-thick $Mn_{1.96}Fe_{0.67}Ga$ changes more rapidly than 10-nm-thick $Mn_{1.96}Fe_{0.67}Ga$, which indicates that antiferromagnetic orders in 5-nm-thick $Mn_{1.96}Fe_{0.67}Ga$ are easy to be reversed by thermal activation. From previous study, antiferromagnetic orders in each grain are subject to be reversed when thermal energy becomes larger than $K_{AF}V$, where $K_{AF}$ is the antiferromagnetic anisotropy and $V$ is its grain volumes [43]. In our results, since 5-nm-thick $Mn_{1.96}Fe_{0.67}Ga$ are thinner than that of 10 nm, its grain volumes are expected to be smaller, which results in low $< T_B >$. Hence, for the further development of this material, $< T_B >$ of $(Mn,Fe)_3Ga$ films can be increased more by growing larger grains with optimizing growth conditions. Also, $< T_B >$ of in-plane (see Fig. 5) and perpendicular exchange bias (see Fig. 9) are almost the same of 235 and 240 K, respectively. This result suggests that $K_{AF}$ of $(Mn,Fe)_3Ga$ with both directions are almost the same.

## 4. Conclusion

We studied the effect of Fe doping into $D0_{19}$ $Mn_3Ga$ films. XRD analysis proves no minor $Mn_2FeGa$ peaks and shifts in (0 0 0 2) and

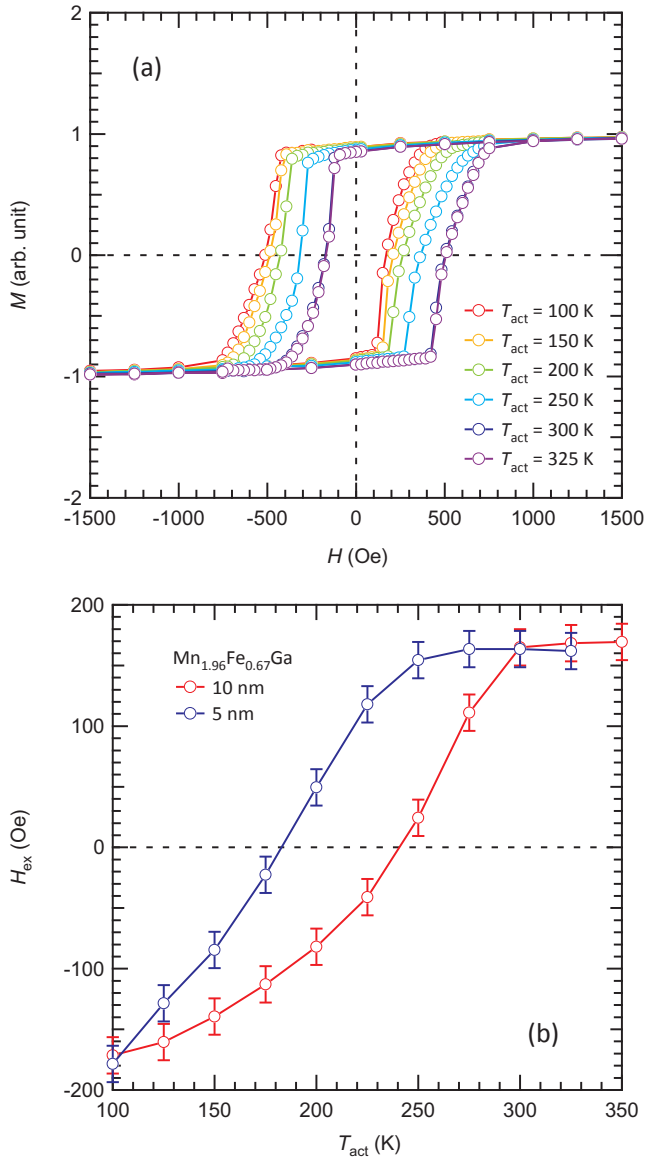


**Fig. 9.** (a) Out-of-plane magnetization curves of the $Mn_{1.96}Fe_{0.67}Ga$ (10)/[Co (1.0)/Pt(1.6)]$_3$ bilayer measured at 100 K after thermal activation at different $T_{act}$ under a reversed magnetic field. (b) $H_{ex}^{perp}$ dependence on $T_{act}$ in $Mn_{1.96}Fe_{0.67}Ga$ (5, 10)/[Co(1.0)/Pt(1.6)]$_3$.

(0 0 0 4) peaks, confirming successful Fe doping of $D0_{19}$ $Mn_3Ga$ films is achieved without inducing an extra crystalline phase. The shifts in magnetic hysteresis loops are detected for both in-plane and out-of-plane magnetization curves by attaching a $Co_{0.6}Fe_{0.4}$ layer and a [Co/Pt]$_3$ multilayer, respectively. In-plane $H_{ex}$ is enhanced up to 446 Oe at 120 K for a $Mn_{1.99}Fe_{0.49}Ga$ film, which is greater than that for $Mn_3Ga$ (299 Oe) as previously reported [27]. Perpendicular $H_{ex}$ is also increased by optimizing the Fe composition and (Mn,Fe)$_3$Ga thickness, achieving the largest perpendicular $H_{ex}$ of 163 Oe for 5-nm-thick $Mn_{1.96}Fe_{0.67}Ga$ film at 120 K. Median blocking temperature of 10-nm-thick $Mn_{1.99}Fe_{0.49}Ga$ and $Mn_{1.96}Fe_{0.67}Ga$ are estimated to be 235 and 240 K for in-plane and perpendicular $H_{ex}$, respectively. This diversity between the in-plane and perpendicular exchange bias is associated with the change in the (Mn,Fe)$_3$Ga spin structure with noncollinear spins as theoretically reported in Ref. [35]. Therefore, our method to control the exchange bias by doping a transition metal can be applied to different antiferromagnetic materials and is very useful to develop antiferromagnetic materials and implement them into a spintronic device.

## Acknowledgements

This study is partially supported by JSPS-EPSRC Core-to-Core programme (EP/M02458X/1). Also, the authors would like to thank M. Oogane for fruitful discussion and J. Gompertz, W. Frost, H. Wu, and J. Sinclair for their experimental support.

## References

[1] W.H. Meiklejohn, C.P. Bean, Phys. Rev. 102 (1956) 1413.
[2] S.A. Wolf, D.D. Awschalom, R.A. Buhrman, J.M. Daughton, S. von Molnár, M.L. Roukes, A.Y. Chtchelkanova, D.M. Treger, Science 294 (2001) 1488.
[3] A. Fert, Rev. Mod. Phys. 80 (2008) 1517.
[4] J. Lenz, A.S. Edelstein, IEEE Sens. J. 6 (2006) 631.
[5] Y. Ando, Jpn. J. Appl. Phys. 54 (2015) 070101.
[6] K. Fujiwara, M. Oogane, A. Kanno, M. Imada, J. Jono, T. Terauchi, T. Okuno, Y. Aritomi, M. Morikawa, M. Tsuchida, N. Nakasato, Y. Ando, Appl. Phys. Express 11 (2018) 023001.
[7] T. Miyazaki, N. Tezuka, J. Magn. Magn. Mater. 139 (1995) L231–L234.
[8] J.S. Moodera, L.R. Kinder, T.M. Wong, R. Meservey, Phys. Rev. Lett. 74 (1995) 3273.
[9] M.N. Baibich, J.M. Broto, A. Fert, F. Nguyen Van Dau, F. Petroff, P. Etienne, G. Creuzet, A. Friederich, J. Chazelas, Phys. Rev. Lett. 61 (1988) 2472.
[10] G. Binasch, P. Grunberg, F. Saurenbach, W. Zinn, Phys. Rev. B 39 (1989) 4828.
[11] B. Dieny, V.S. Speriosu, S. Metin, S.S.P. Parkin, B.A. Gurney, P. Baumgart, D.R. Wilhoit, J. Appl. Phys. 69 (1991) 4774.
[12] https://ec.europa.eu/growth/sectors/raw-materials/specific-interest/critical_en.
[13] A. Hirohata, T. Huminiuc, J. Sinclair, H. Wu, M. Samiepour, G. Vallejo-Fernandez, K. O'Grady, J. Balluf, M. Meinert, G. Reiss, E. Simon, S. Khmelevskyi, L. Szunyogh, R.Y. Díaz, U. Nowak, T. Tsuchiya, T. Sugiyama, T. Kubota, K. Takanashi, N. Inami, K. Ono, J. Phys. D : Appl. Phys. 50 (2017) 443001.
[14] I. Galanakis, P.H. Dederichs, Phys. Rev. B 66 (2002) 174429.
[15] H. Wu, G. Vallejo-Fernandez, A. Hirohata, J. Phys. D: Appl. Phys. 50 (2017) 375001.
[16] T. Tsuchiya, R. Kobayashi, T. Kubota, K. Saito, K. Ono, T. Ohhara, A. Nakao, K. Takanashi, J. Phys. D: Appl. Phys. 51 (2018) 065001.
[17] D. Zhang, B. Yan, S.-C. Wu, J. Kubler, G. Kreiner, S.S.P. Parkin, C. Felser, J. Phys.: Condens. Matter 25 (2013) 206006.
[18] E. Kren, G. Kadar, Solid State Commun. 8 (1970) 1653.
[19] S. Tomiyoshi, Y. Yamaguchi, T. Nagamiya, J. Magn. Magn. Mater. 31 (1983) 629.
[20] I. Dzyaloshinskii, J. Phys. Chem. Solids 4 (1958) 241.
[21] T. Moriya, Phys. Rev. Lett. 4 (1960) 228.
[22] S. Nakatsuji, N. Kiyohara, T. Higo, Nature 527 (2015) 212.
[23] N. Kiyohara, T. Tomita, S. Nakatsuji, Phys. Rev. Appl. 5 (2016) 064009.
[24] Z.H. Liu, Y.J. Zhang, G.D. Liu, B. Ding, E.K. Liu, Hasnain Mehdi Jafri, Z.P. Hou, W.H. Wang, X.Q. Ma, G.H. Wu, Sci. Rep. 7 (2017) 515.
[25] H. Kurt, K. Rode, M. Venkatesan, P. Stamenov, J.M.D. Coey, Phys. Status Solidi B 248 (2011) 2338.
[26] H. Kurt, K. Rode, H. Tokuc, P. Stamenov, M. Venkatesan, J.M.D. Coey, Appl. Phys. Lett. 101 (2012) 232402.
[27] H. Wu, I. Sudoh, R. Xu, W. Si, C.A.F. Vaz, J.-Y. Kim, G. Vallejo-Fernandez, A. Hirohata, J. Phys. D: Appl. Phys. 51 (2018) 215003.
[28] T. Ogasawara, J.-Y. Kim, Y. Ando, A. Hirohata, J. Magn. Magn. Mater. 473 (2019) 7.
[29] A. Markou, J.M. Taylor, A. Kalache, P. Werner, S.S.P. Parkin, C. Felser, Phys. Rev. Mater. 2 (2018) 051001.
[30] S. Maat, K. Takano, S.S.P. Parkin, Eric E. Fullerton, Phys. Rev. Lett. 87 (2001) 087202.
[31] F. Garcia, G. Casali, S. Auffret, B. Rodmacq, B. Dieny, J. Appl. Phys. 91 (2002) 6905.
[32] Z.Y. Liu, S. Adenwalla, J. Appl. Phys. 94 (2003) 1105.
[33] J. Sort, V. Baltz, F. Garcia, B. Rodmacq, B. Dieny, Phys. Rev. B 71 (2005) 054411.
[34] P. Zilske, D. Graulich, M. Dunz, M. Meinert, Appl. Phys. Lett. 110 (2017) 192402.
[35] A. Kundu, S. Ghosh, Intermetallics 93 (2018) 209.
[36] K. Minakuchi, R.Y. Umetsu, K. Ishida, R. Kainuma, J. Alloys Compd. 537 (2012) 332.
[37] Z.H. Liu, Y.J. Zhang, H.G. Zhang, X.J. Zhang, X.Q. Ma, Appl. Phys. Lett. 109 (2016) 032408.
[38] E. Krén, G. Kádár, Solid State Commun. 8 (1971) 1653.
[39] H. Ohldag, A. Scholl, F. Nolting, E. Arenholz, S. Maat, A.T. Young, M. Carey, J. Stöhr, Phys. Rev. Lett. 91 (2003) 017203.
[40] P. Kappenberger, S. Martin, Y. Pellmont, H.J. Hug, J.B. Kortright, O. Hellwig, E.E. Fullerton, Phys. Rev. Lett. 91 (2003) 267202.
[41] Z.M. Tian, S. Huang, Y. Qiu, S.L. Yuan, Y.Y. Wu, L. Li, J. Appl. Phys. 113 (2013) 143906.
[42] G. Vallejo-Fernandez, L.E. Fernandez-Outon, K. O'Grady, J. Phys. D: Appl. Phys. 41 (2008) 112001.
[43] K. O'Grady, L.E. Fernandez-Outon, G. Vallejo-Fernandez, J. Magn. Magn. Mater. 322 (2010) 883.
[44] M. Tsunoda, H. Takahashi, M. Takahashi, IEEE Trans. Magn. 45 (2009) 3877.